Influence of Deposition Temperatures on the Structural and Optical Properties of Zn_2SnO_4 (ZTO) Thin Films

Layth A. Saleh[1*], Ziad T. Khodair[2]

Abstract

In this paper, the structural and optical properties of Zn_2SnO_4 thin films were studied. Chemical spray pyrolysis was used to make the films on glass substrates at varying temperatures (450, 500, and 550˚C). All samples have a polycrystalline structure with a cubic spinel structure, according to XRD studies. Field emission scanning electron microscopy (FE-SEM) investigated surface morphology, and AFM stands for atomic force microscopy. After increasing the temperature, the surface roughness and mean grain size both increased. In the wavelength range of 300-1100 nm, optical characteristics were examined as a function of wavelength because of crystal formation. The absorption spectra of Zn_2SnO_4 thin films reveal that absorption decreases with increasing temperature for all samples. The optical properties of the material, such as the extinction coefficient, refractive index, and dielectric constant, were investigated as well.

Key Words: Zn_2SnO_4 Thin Film, XRD, Spray Pyrolysis, Optical Properties, Structural Properties, AFM.

DOI Number: 10.14704/nq.2022.20.4.NQ22107 **NeuroQuantology 2022; 20(4):159-167**

Introduction

It has been demonstrated that zinc stannate Zn_2SnO_4, also known as zinc tin oxide (ZTO), has high electron mobility (10-15 $cm^2/V.s$). Zn_2SnO_4 is an n-type transparent conductive oxide with a broad band gap of 3.6 eV and high electrical conductivity (Li *et al.*, 2012), (Abood *et al.*, 2020). It has excellent visual optical qualities and can be employed. Solar cells, for example, are used in a range of applications, moisture sensors and combustible gas sensors. (Li *et al.*, 2012), (Abood *et al.*, 2020). In recent decades, its applications have expanded to include gas sensing devices and solar cells (Zeng et al., 2009), (Lana-Villarreal, Boschloo and Hagfeldt, 2007), Li-ion batteries and photocatalysts for pollution treatment (Divya, Jaya and Pradyumnan, 2014). Nonetheless, a few attempts have been made to manufacture thin films ZTO using the spray pyrolysis technique (Farhan, Khodair and Ibrahim, 2020), (Khodair, Ibrahim and Hassan, 2020). This allows the qualities of the final material to be fine-tuned.

Corresponding author: Layth A. Saleh

Address: [1*]Department of Physics, College of Science, University of Diyala, Diyala, Iraq; [2]Department of Physics, College of Science, University of Diyala, Diyala, Iraq.

[1*]E-mail: lyth34605@gmail.com

[2]E-mail: ziad_tariq70@yhoo.com

Relevant conflicts of interest/financial disclosures: The authors declare that the research was conducted in the absence of any commercial or financial relationships that could be construed as a potential conflict of interest.

Received: 12 February 2022 **Accepted:** 20 March 2022

A multi-component system offers an aggregation of features of distinct participating atoms to favour their stability in hostile chemical conditions, in addition to being adaptable. Zn-Sn-O is thought to offer potential optical and electrical qualities as a TCO material among the different ternary oxides available. Zn_2SnO_4 (cubic spinel) and $ZnSnO_3$ (orthorhombic) are the two crystallographic phases of zinc stannate, comprising ZnO and SnO_2. The visible spectrum is great transparency (Sinha et al., 2011), (Wang et al., 2017), (Tharsika, Haseeb and Sabri, 2014) We are currently study the structural and optical properties of Zn_2SnO_4 thin films formed on a glass slide using spray pyrolysis technique because of their significant advantages in terms of equipment simplicity and film formation control. Huge quantities and large areas of thin films are easily handled. (Vijayalakshmi et al., 2008).

Experimental Procedure

The thin films of zinc stannite were made using the spray pyrolysis setup previously described (Hameed et al., 2021), (Khodair et al., 2020). An aqueous solution was made by pulverizing $Zn(NO_3)_2.4H_2O$. $2H_2O$, and $SnCl_2$ to $2H_2O$, in the molar ratio, (1:1) in 100 ml of the water This solution was put on a magnetic stirrer with heating for 30 mints with addition dropped from (HCl) to ensure the perfect solubility with water. The result solution was transparent and homogenous the deposition process was carried out at temperatures of at (450, 500 and 550°C). Then the samples were transferred to the oven for heat treatment at temperatures (450, 500 and 550°C) to get improve crystallity and (1.5×10^{-5} Nm^{-2}) is the pressure that was employed. The distance between the nozzle and the sprayed substrate is (31 cm), and the spray period is (60 seconds). They were allowed to cool at ambient temperature slowly. The thickness of the thin film was measured using the cross-section method (290nm).

Results and Discussion

X-ray diffraction techniques were used to investigate the crystalline structure of Zn_2SnO_4 thin films produced on glass slides by spray pyrolysis deposition at (450, 500 and 550°C) temperatures. The average crystallite size was determined using Scherrer formula (Abed et al., 2019).

$$D_{av} = \frac{K\,\lambda}{\beta cos\theta} \quad (1)$$

Where θ: is the Bragg's angle of the XRD Peak.

K: - the shape factor, which is determined by the material's shape and its value within a given range (0.9-1).

β: Full Width at Half Maximum (FWHM) measured in radians.

Figure (1) represents the X-ray diffraction (XRD) patterns of Zn_2SnO_4 thin films of different deposit temperatures (450,500 and 550°C). We can observe that the deposition films have a polycrystalline structure prepared by the spray pyrolysis method. Zn_2SnO_4 thin film a deposit at (450,500 and 550)°C shows five diffraction peaks at 2θ values of (29.6436°, 34.6851°, 36.4354°, 41.0518° and 60.9610°). These were assigned to the diffraction lines produced by (220), (311), (222), (400) and (440) of the (cubic spinel) structure of Zn_2SnO_4 confirmed by standard data. Many more peaks can be seen in the XRD pattern for the hexagonal ZnO at 2θ values of (31.9992°, 47.7467°, 56.6877° and 62.2236°) and tetragonal SnO_2 at 2θ values of (26.6052°, 37.6160° and 51.4990°). The strongest peak located at 2θ values (~34°) corresponding to (311) direction respect to Zn_2SnO_4 crystals. The FWHM decreases as the deposition temperature rises, indicating that particle size is increasing. The intensity of the peaks increases as the substrate temperature increases, which means that the crystallization of the film improves as the temperature of the deposition increases. The deposition process reduces crystalline defects and reduces optical dispersion. Table 1 shows the experiment peaks from (ICDD Joint Committee on Powder Diffraction Standards - (ICDD) International Centre for Diffraction Data) cards number (24-1470, 96-210-4744 and 96-901-1663) Returns to Zn_2SnO_4, SnO_2 and ZnO Respectively.

Table 1. Structural parameters: Inter-planar spacing, crystalline size of Zn_2SnO_4 films

Temperature (°C)	2Θ (Deg.)	FWHM (Deg.)	d_{hkl} (Å)	D_{ave} (nm)	hkl	Phase	Card no.
450	26.6478	0.61140	3.41794	13.35	110	SnO_2	96-210-4744
	29.6436	0.70360	3.01116	11.68	220	Zn_2SnO_4	24-1470
	31.9992	0.70390	2.79468	11.74	100	Hex. ZnO	96-901-1663
	34.6851	0.75910	2.58417	10.96	311	Zn_2SnO_4	24-1470
	36.4354	0.74290	2.46395	11.26	222	Zn_2SnO_4	24-1470
	37.6160	0.51760	2.41279	16.22	200	SnO_2	96-210-4744
	41.0518	0.76250	2.19690	11.13	400	Zn_2SnO_4	24-1470
	47.7467	0.80150	1.90331	10.48	102	Hex. ZnO	96-901-1665
	51.4990	0.73340	1.77310	12.03	211	SnO_2	96-210-4744
	56.6877	0.89360	1.62250	10.10	110	Hex. ZnO	96-901-1663
	60.9610	1.68570	1.56525	5.47	440	Zn_2SnO_4	24-1470
	62.2236	0.56660	1.49078	16.38	103	Hex. ZnO	96-901-1663
500	26.6454	0.54290	3.31806	15.04	110	SnO_2	96-210-4744
	29.6127	0.70154	3.04327	11.71	220	Zn_2SnO_4	24-1470
	31.9132	0.67380	2.80202	12.26	100	Hex. ZnO	96-901-1663
	34.6109	0.70080	2.58954	11.87	311	Zn_2SnO_4	24-1470
	36.4014	0.71660	2.46617	11.67	222	Zn_2SnO_4	24-1470
	37.6365	0.46990	2.38808	17.86	200	SnO_2	96-210-4744
	41.6458	0.73740	2.16639	11.53	440	Zn_2SnO_4	24-1470
	47.6334	1.00060	1.90757	8.68	102	Hex. ZnO	96-901-1665
	51.4442	0.66000	1.77486	13.36	211	SnO_2	96-210-4744
	56.6224	0.70610	1.62421	12.78	110	Hex. ZnO	96-901-1663
	60.3810	1.07270	1.50921	8.57	440	Zn_2SnO_4	24-1470
	62.9797	0.67780	1.47469	13.75	103	Hex. ZnO	96-901-1663
550	26.6052	0.51249	3.31127	15.93	110	SnO_2	96-210-4744
	29.60365	0.70125	3.01325	11.72	220	Zn_2SnO_4	24-1470
	31.6749	0.4920	2.82740	16.79	100	Hex. ZnO	96-901-1663
	34.3810	0.3936	2.60969	21.13	311	Zn_2SnO_4	24-1470
	36.1929	0.3936	2.48606	21.24	222	Zn_2SnO_4	24-1470
	37.7240	0.40670	2.41279	20.65	200	SnO_2	96-210-4744
	41.3655	0.66754	2.16731	7212.	400	Zn_2SnO_4	24-1470
	47.367	0.6853	1.91768	12.66	102	Hex. ZnO	96-901-1665
	51.5903	0.59286	1.77310	14.85	211	SnO_2	96-210-4744
	56.3123	0.6074	1.63240	14.90	110	Hex. ZnO	96-901-1663
	60.3376	0.97690	1.51674	9.41	440	Zn_2SnO_4	24-1470
	62.645	0.6365	1.48175	14.61	103	Hex. ZnO	96-901-1663

Atomic Force Microscope (AFM)

The surface morphology of deposited Zn_2SnO_4 films with various temperatures (450, 500 and 550°C) was examined by AFM, as shown in Fig. 2. Average roughness and RMS are increased with increased substrate temperature. This could be attributed to larger clusters resulting from the coalescence of two or more grains and a decrease or removal of grain bounders. It can be seen from (Table 2) that the Average Diameter increased with increased temperature, which is in agreement with (Coutts et al., 2000).

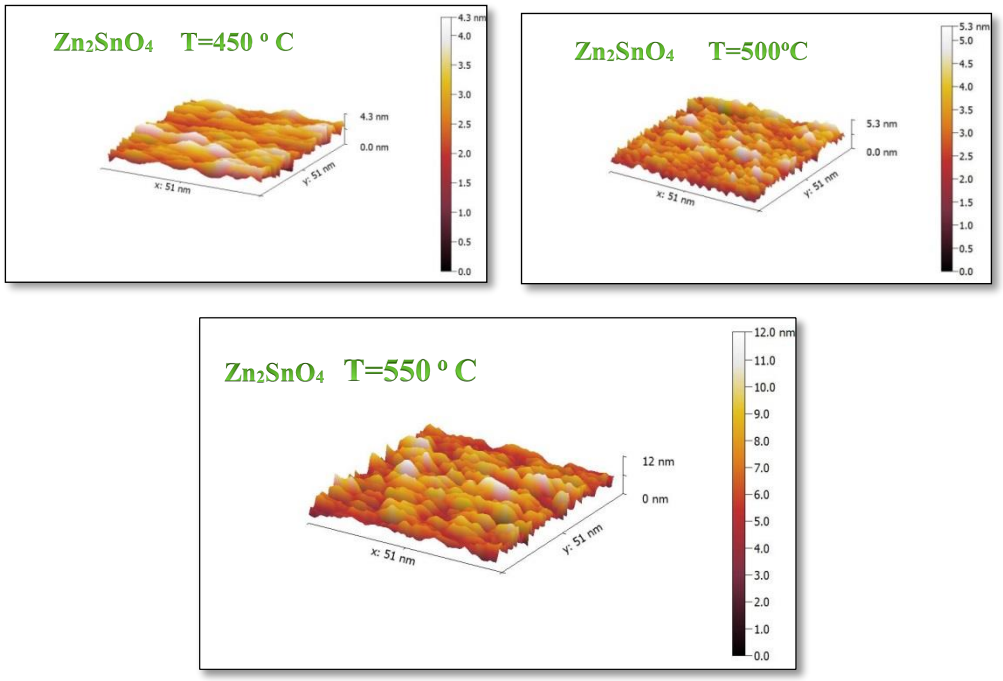

Figure 2. AFM images for Zn_2SnO_4 films at different substrate temperatures (450,500 and 550˚C)

Table 2. AFM parameters (Average Diameter, roughness Average and RMS) for Zn_2SnO_4 films at temperatures (450,500 and 550˚C).

Temperature ˚C	Average Diameter (nm)	Roughness Average (nm)	RMS (nm)
450	6.387	1.632	1.979
500	12.22	1.969	2.416
550	17.87	3.886	4.608

Field Emission-Scanning Electron Microscopy (FE-SEM)

Field Emission Scanning Electron Microscope The (FE-SEM) method was utilized to study the morphology of the surface and microstructure features of deposit thin film. To study the surface of zinc stannite thin films, FE-SEM images of obtained samples for zinc stannite thin films were taken. Figure (3. A) shows the FE-SEM picture of the zinc stannite deposited at temperature (450°C), and Figure (3-B) depicts that because the particles were created on the nanoscale, their sizes ranged from 11.13nm to 36.74nm, with an average diameter of 22.14nm and a nearly spherical uniform distribution.

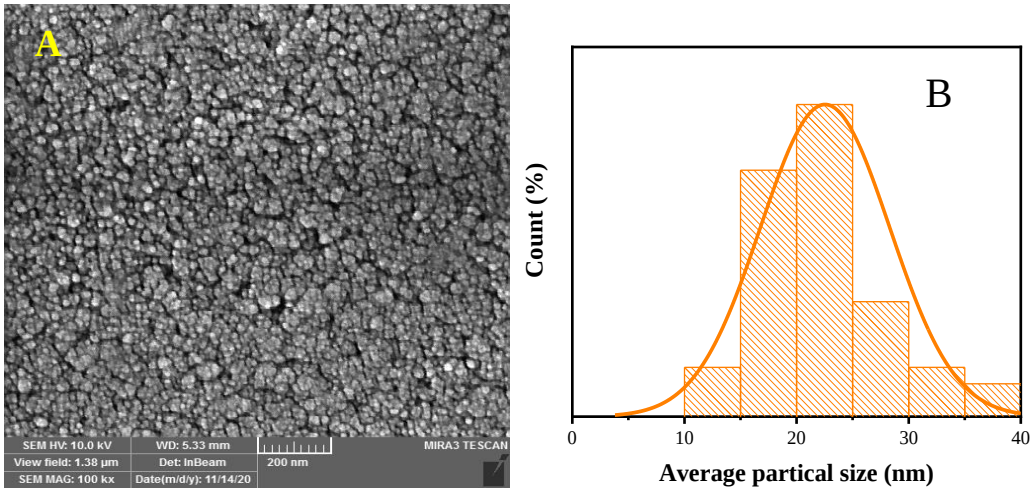

Figure (3. A). Zn_2SnO_4 thin film deposit at (450°C) temperature (A) FE-SEM picture (3-B). Volumetric distribution thin film

Figure (3. A) shows an FE-SEM image of stannite deposited at 500°C, and Figure (3-B) shows that the particles were obtained on the Nanoscale, with sizes ranging from (11.14-39.90) nm at a rate of average diameters (23.92 nm), and that with higher substrate temperatures, the particles shifted to hexagonal granule shapes.

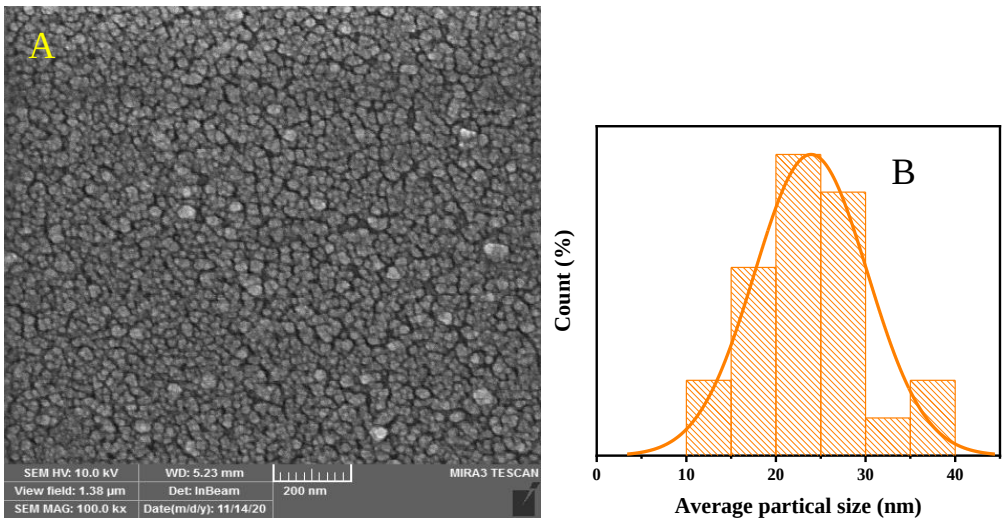

Figure (3. A). Zn_2SnO_4 thin film deposit at (500°C) temperature (A) FE-SEM picture (3-B). Volumetric distribution thin film

Figure (3. A) shows the FE-SEM picture of the stannite deposit at a temperature (550°C), and Figure (3-B) shows the particles were obtained within the Nanoscale. The sizes ranged between (8.21-60.82) nm at a rate of the average diameters (33.58 nm) which shifted to small stones shapes with higher deposition temperatures.

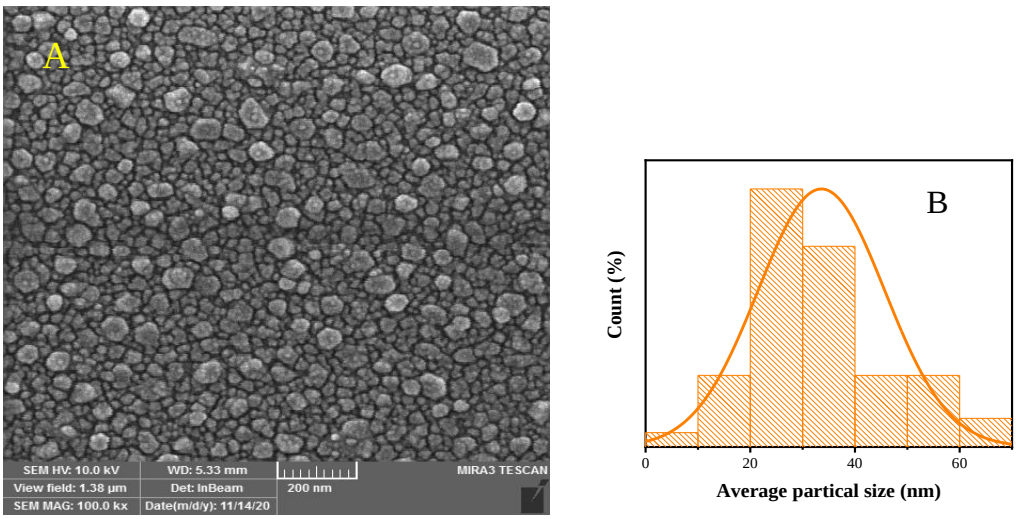

Figure (3. A). Zn_2SnO_4 thin film deposit at (550°C) temperature (A) FE-SEM picture (3-B). Volumetric distribution thin film

The average size of aggregated particles increases noticeably after the temperature increase. This result could be attributed to increased atom mobility as temperature rises, resulting in more effective recrystallization and grain growth in the films, resulting in larger grains. This result matched the findings of (Gu et al., 2021).

Optical Properties

The crystalline structure, thickness, and type of materials used all influence the optical properties of thin films. In the range of (200-1100) nm, the optical properties were investigated using a UV-visible spectral spectrometer (SP-8001). All-optical constants are measured using the output data from the absorption, wavelength, and transmitter in a

computer program. The optical energy gap (Eg) for allowed direct electronic transitions of Zn_2SnO_4 thin film was calculated from the following equation (Vijayalakshmi et al., 2008):

$$\alpha h\nu = A(h\nu - Eg)^r \quad (2)$$

Where (hν) is the photon energy, *A* is a constant that depends on the effective mass and the refractive index, E_g is the energy gap, and (*r*) is constant. Its value depends on the transition nature, where r = 1/2 for direct allowed transitions and r = 3/2 for direct forbidden transitions.

The extinction coefficient (k_o) was estimated by (Khodair et al., 2020).

$$k_o = \frac{\alpha\lambda}{4\pi} \quad (3)$$

We can learn about the behavior of the ZTO's refractive index spectra n_o and extinction k_o by measuring absorption and transmittance spectra.

$$n_o = \left(\frac{4R}{(R-1)^2} - k^2\right)^{1/2} - \frac{(R+1)}{(R-1)} \quad (4)$$

Where R is the reflectance and (k) is the extinction coefficient, the behavior of (n_o) corresponds to the reflectance (Ibrahim, Khodiar and Farhan, 2021).

The real and imaginary part of the dielectric constant can be calculated by using the following equations (Abdel-Aziz et al., 2006):

$$\varepsilon_r = n^2 - k^2 \quad (5)$$

$$\varepsilon_i = 2nk \quad (6)$$

Fig. 4 shows the absorption spectrum as a function of the wavelength for a range (300-900) nm. It can be seen that as the deposition temperature rises, the amount of absorption decreases as a result of increased crystallization. This is because within the forbidden energy gap and conduction band, donor levels (i.e. localized states) decay and disappear. This leads to an increase in the value of E_g. Near UV-visible light region, a strong photo-absorption at a wavelength of 400 nm at 450°C, 385nm at 500°C and 381nm at 550°C are presented. This result is in agreement with (Abood *et al.*, 2020).

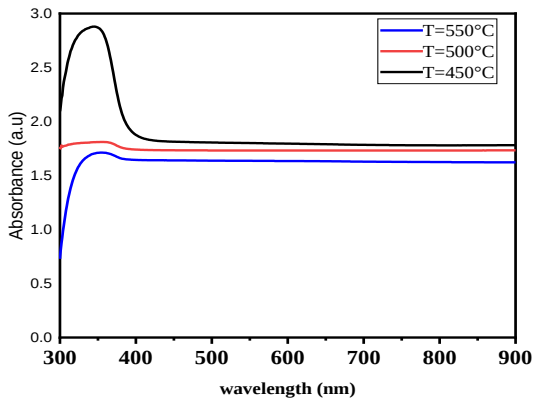

Figure 4. The absorbance for Zn_2SnO_4 thin films at different substrates temperature (450,500 and 550 °C)

The absorption coefficient of (Zn_2SnO_4) nanostructures thin films was calculated by the following equation(7) (Khodair, Ibrahim and Hassan, 2020).

$$\alpha = 2.303\frac{A}{t} \quad (7)$$

where: A: Absorption, t: the thickness of the film (cm).

Fig. 5 shows the optical absorption coefficient α as a function of wavelength (λ) for Zn_2SnO_4 thin films. It is clear from Figure 5 that the values of α become higher ($\alpha > 10^5$) cm^{-1}, implying that a direct electronic transition occurs in these regions. In addition, we found that the value of α from the Zn_2SnO_4 films has a strong absorption coefficient at the short wavelength region (high energies). On the other hand, it is found that the value of α decreases with increasing substrate temperature due to increasing energy gap E_g. The values of α are approximately equal to the reported values by (Abood *et al.*, 2020).

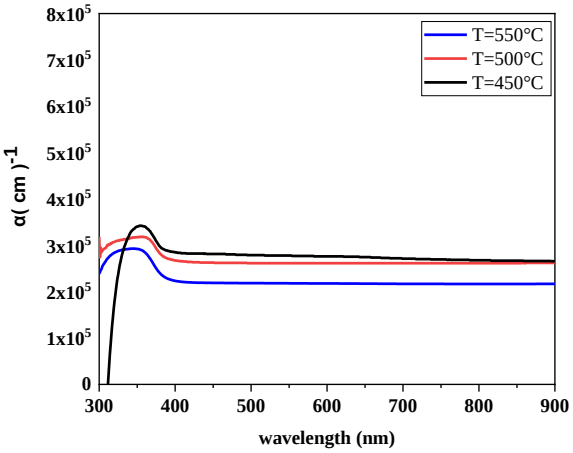

Figure 5. The Absorption Coefficient for Zn_2SnO_4 thin films at different substrates temperature (450,500 and 550°C)

The values of the optical energy gap E_g for nanoparticles Zn_2SnO_4 thin films are determined using eq (2); A plot of relation $(\alpha h\nu)^2$ versus photon energy (hν) and the choice of the desired linear section. From Fig.6, it is clear that the energy gap increased from (3.20-3.30) eV due to the increasing substrate temperature. This is due to the growth of grain size and the reduction of the number of grain boundaries. A rise in Eg may improve crystal structures due to reduced absorption, which reduces defects (tail state) in the forbidden gap, increasing Eg. The values of the approximate absorption coefficient were reprted by (Li et al., 2011).

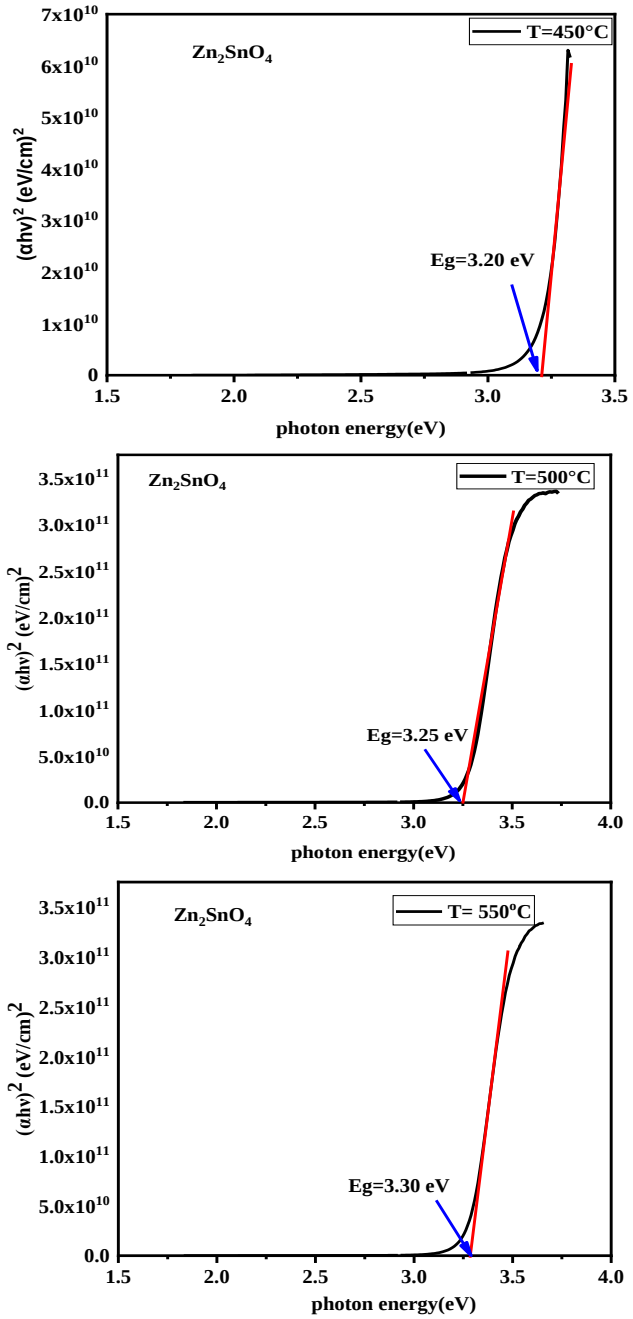

Figure 6. $(\alpha h\nu)^2$ as a function of photon energy for Zn_2SnO_4 films prepared at different substrates temperatures a (450, 500, and 550˚C)

According to formula (3), the behaviour of the extinction coefficient (K) is similar to the behaviour of the absorption coefficient (α). Fig. 7 shows the extinction coefficient (K) as a function of the wavelength (λ) of Zn_2SnO_4 films at (450, 500, 550) ˚C. The extinction coefficient (K) decreases with increasing temperature, as shown in Figure 7 and Table 3. This result is consistent (Mohammed, Aadim and Ameen, 2018).

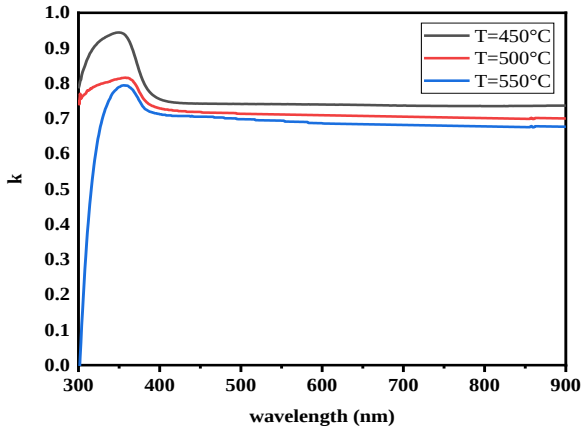

Figure 7. The Extinction coefficient for nanostructure Zn_2SnO_4 films deposited at different substrates temperatures (450,500 and 500˚C)

As shown in Fig. 8, the refractive index (n) value for all films is approximately limited by (2-2.5). We can see from these graphs that (n) increases slightly as the substrate temperature rises. The reason for this is twofold: first, grain size increases, which leads to increased Surface roughness and reflection, which affects the refractive index. Second, temperature increase reduces the porosity and increases the density of thin films, which reduces the light velocity and causes a change in the refractive index. The results are consistent with (Mohammed, Aadim and Ameen, 2018).

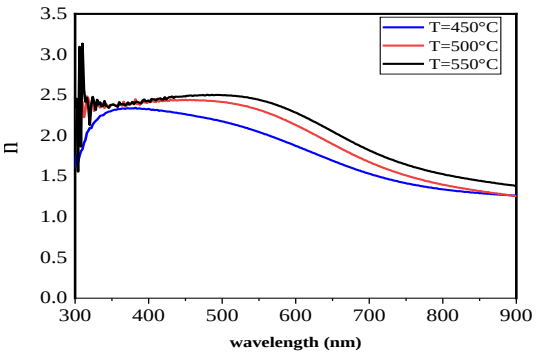

Figure 8. The Refractive Index for Zn_2SnO_4 films prepared at different substrates temperatures (450, 500, and 550˚C)

The electrical dielectric constant was studied in real and imaginary parts as a function of wavelength. Fig. 9 (a) shows the relationship between the real portion of the dielectric constant versus the wavelength where we see that all samples behave like refractive index (n) samples due to the small value of (k^2) compared to (n^2) based on eq. (5) Fig. 9 (b) shows the relationship between the imaginary portion of the dielectric constant versus the wavelength. We found that all samples behave like extinction coefficients (k) based on equation (6). This means that as the substrate temperature rises,

the real part rises, and the value of the imaginary part decreases as the temperature rises. It can be observed that the values of the real portion of the dielectric constant decrease with increasing wavelengths, and actual values of the real part are more significant than the values of the imaginary part, as shown in Table 3. These measurements correspond with (Salohub et al., 2017), (Satoh et al., 2004).

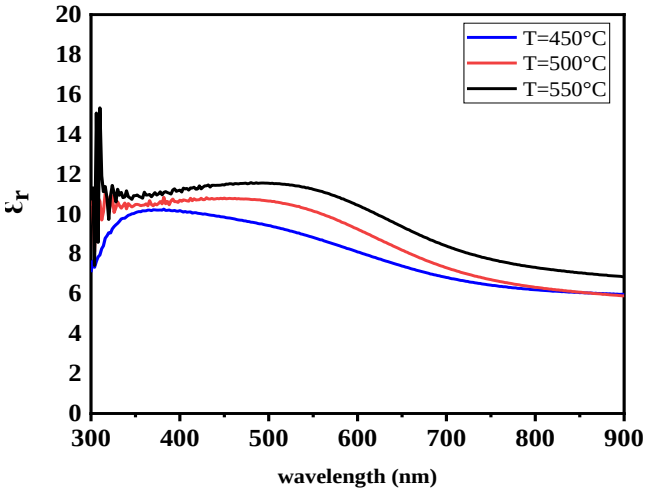

Figure 9(a). The Real Part of Dielectric Constants of Zn_2SnO_4 Films prepared at different substrates temperatures (450, 500, and 550˚C)

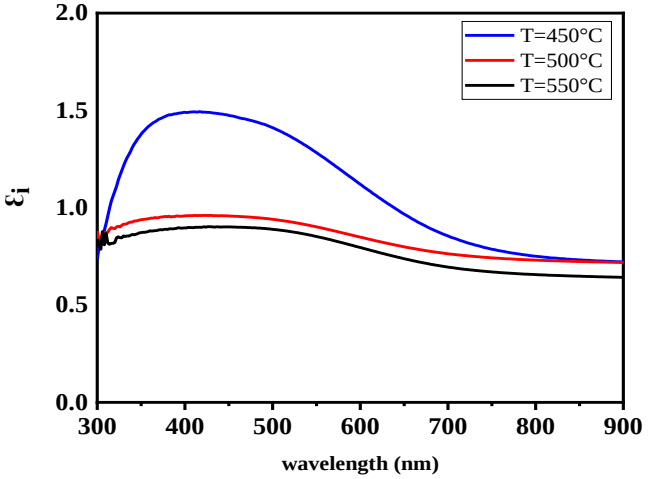

Figure 9(b). The Imaginary Part of Dielectric Constants of Zn_2SnO_4 Films prepared at different substrates temperatures (450, 500, and 550 ˚C)

Table 3. Values of Optical Properties for Zn_2SnO_4 films (at 500 nm wavelength) and The Optical Energy Gap (E_g)

Temperature ˚C	α $(cm)^{-1}$	k◦	n◦	ε_r	ε_i	E_g (eV)
450	28364	0.78	2.18	9.40	1.427	3.02
500	26146	0.74	2.41	10.75	0.945	3.11
550	22320	0.70	2.50	11.61	0.885	3.22

Conclusion

The spray deposition technique is a suitable approach for the deposition of Zn_2SnO_4 thin films on glass substrates; according to structural and optical properties, the post-heat treatment procedure aids in the improvement of thin film crystalline quality. The films are all polycrystalline with a cubic spinel nanostructure. According to XRD, AFM, and FE-SEM, the average diameter, roughness average, and RMS of the nanoparticle's thin-film increase with increasing the substrate temperature. The direct energy band gap values increase, reaching 3.30 eV for the film deposited at 550 ˚C.

References

Abdel-Aziz, M.M. *et al.* (2006). Determination and analysis of dispersive optical constant of TiO2 and Ti2O3 thin films', *Applied surface science*, 252(23), 8163–8170.

Abed, A.H. *et al.* (2019) 'Study the evaluation of Williamson–Hall (WH) strain distribution in silver nanoparticles prepared by sol-gel method', in *AIP Conference Proceedings*. AIP Publishing LLC, 20019.

Abood, A.T. *et al.* (2020). 'Structural and optical properties of nanocrystalline SnO_2 thin films growth by electron beam evaporation', in *AIP Conference Proceedings*. AIP Publishing LLC, 20036.

Baruah, S., & Dutta, J. (2011). 'Zinc stannate nanostructures: hydrothermal synthesis', *Science and technology of advanced materials*.

Coutts, T.J. *et al.* (2000). 'Search for improved transparent conducting oxides: A fundamental investigation of CdO, Cd_2SnO_4, and Zn_2SnO_4', *Journal of Vacuum Science & Technology A: Vacuum, Surfaces, and Films*, 18(6), pp. 2646–2660.

Divya, N.K., Jaya, T.P. and Pradyumnan, P.P. (2014). 'Variation in Morphology and crystallinity of ZTO ceramics', *Research Journal of Recent Sciences ISSN*, 2277, 2502.

Farhan, M.M., Khodair, Z.T. and Ibrahim, B.A. (2020). 'Study of the Structural and Optical Properties of Ni-doped Co_3O_4 Thin Films Using Chemical Spray Pyrolysis Technique', in *IOP Conference Series: Materials Science and Engineering*. IOP Publishing, 12090.

Gu, Y. *et al.* (2021). 'Nonlinear growth of zinc tin oxide thin films prepared by atomic layer deposition', *Ceramics International*, 47(16), 22760–22767.

Hameed, S.A. *et al.* (2021) 'The influence of deposition temperatures on the structural and optical properties for NiO nanostructured thin films prepared via spray pyrolysis technique', *Chemical Data Collections*, 33, 100677.

Ibrahim, B.A., Khodiar, Z.T. and Farhan, M.M. (2021). 'Study of some Physical Properties and the Effect of Gamma Irradiation on Optical Properties of Electrochromic Co_3O_4 Thin Film', in *Materials Science Forum*. Trans Tech Publ, 107–114.

Khodair, Z.T. *et al.* (2020). 'Study of optical and structural properties of (NiO) 1-x (CuO) x nanostructures thin films', *Chemical Data Collections*, 28, 100414.

Khodair, Z.T., Ibrahim, B.A. and Hassan, M.K. (2020). 'Investigation on the structural and optical properties of

copper doped NiO nanostructures thin films', *Materials Today: Proceedings*, 20, 560–565.

Lana-Villarreal, T., Boschloo, G. and Hagfeldt, A. (2007) 'Nanostructured zinc stannate as semiconductor working electrodes for dye-sensitized solar cells', *The Journal of Physical Chemistry C*, 111(14), 5549–5556.

Li, Y. *et al.* (2011). 'CdS quantum-dot-sensitized Zn2SnO4 solar cell', *Electrochimica acta*, 56(13), 4902–4906.

Li, Z. *et al.* (2012). 'Vertically building Zn 2 SnO 4 nanowire arrays on stainless steel mesh toward fabrication of large-area, flexible dye-sensitized solar cells', *Nanoscale*, 4(11), 3490–3494.

Mohammed, S.J., Aadim, K.A., & Ameen, M.M. (2018). 'Effect of Annealing on Some Properties of Zn2SnO4 Thin Films Prepared by PLD Technique', *Kirkuk university journal for scientific studies*, 13(4).

Salohub, A.O. *et al.* (2017). 'Determination of fundamental optical constant of Zn_2SnO_4 films', *Semiconductor physics, quantum electronics & optoelectronics*, (20, № 1), 79–84.

Satoh, K. *et al.* (2004) 'Influence of oxygen flow ratio on properties of Zn_2SnO_4 thin films deposited by RF magnetron sputtering', *Japanese journal of applied physics*, 44(1L), L34.

Sinha, S.K. *et al.* (2011). 'Characterization of ZnO–SnO2 thin film composites prepared by pulsed laser deposition', *Applied surface science*, 257(24), 10551–10556.

Tharsika, T., Haseeb, A. and Sabri, M.F.M. (2014). 'Structural and optical properties of $ZnO–SnO_2$ mixed thin films deposited by spray pyrolysis', *Thin Solid Films*, 558, 283–288.

Vijayalakshmi, S. *et al.* (2008) 'Physical properties of zinc doped tin oxide films prepared by spray pyrolysis technique', *Journal of Physics D: Applied Physics*, 41(3), 35505.

Wang, P. *et al.* (2017). 'Stabilization of organometal halide perovskite films by SnO_2 coating with inactive surface hydroxyl groups on ZnO nanorods', *Journal of Power Sources*, 339, 51–60.

Zeng, Y. *et al.* (2009). 'Growth and selective acetone detection based on ZnO nanorod arrays', *Sensors and Actuators B: Chemical*, 143(1), 93–98.